International Journal of Microwave and Wireless Technologies

cambridge.org/mrf

High-order-mode cavity fed 45° linear polarized antenna for 5G applications

Yutong Yang, Zihang Qi, Wenyu Zhao, Genqiang Kou and Xiuping Li

State Key Laboratory of Information Photonics and Optical Communications, the Key Laboratory of Universal Wireless Communications of Ministry of Education, Beijing Key Laboratory of Work Safety Intelligent Monitoring, the School of Electronic Engineering, Beijing University of Posts and Telecommunications, Beijing 100876, China

Research Paper

Cite this article: Yang Y, Qi Z, Zhao W, Kou G, Li X (2024) High-order-mode cavity fed 45° linear polarized antenna for 5G applications. *International Journal of Microwave and Wireless Technologies* **16**(9), 1570–1578. https://doi.org/10.1017/S1759078724001028

Received: 17 April 2024
Revised: 9 September 2024
Accepted: 15 September 2024

Keywords:
45° linear polarization; high-order-mode cavity; low-profile; substrate integrated waveguide; wide bandwidth

Corresponding author: Zihang Qi;
Email: qizihang@bupt.edu.cn

Abstract

In this paper, a high-order-mode (HOM) (TE_{330}) cavity-fed 45° linear polarized 6×6 slot array antenna is proposed. The 45° linear polarization is achieved by introducing asymmetric cross slots on the HOM cavity, resulting in low profile and wide bandwidth. The antenna array was verified using standard printed circuit board technology. Measured results show that the impedance bandwidth ($|S_{11}| \leq -10$ dB) is 13.9% (36.98–42.92 GHz), and the peak gain is 19.3 dBi with a 3-dB gain bandwidth of 13.6%. Attributed to its simple structure, low profile, and wide bandwidth, the presented antenna is a good candidate for 5G applications.

Introduction

Recently, millimeter-wave bands have been used to improve the overall system performance [1, 2, 6, 7]. For radar detection and the fifth generation mobile communications (5G), higher transmission quality can be achieved through improving anti-interference ability in certain specific situations. 45° linear polarized antennas facilitate advanced beamforming and beam steering techniques, allowing precise beam direction toward users, improving signal strength, and reducing interference, which have been extensively employed in practical communications [3, 4, 9, 23]. Moreover, they find applications in high-resolution radar systems for security and surveillance, providing detailed imagery and enhanced detection capabilities [5, 16].

Loading an additional layer between the feed network and the radiation part and increasing the thickness of the radiation slots are the main methods for achieving 45° linearly polarized hollow-waveguide-fed array antennas [3, 8, 9]. In [3], the hollow-waveguide-fed array antenna is proposed with a high cross-polarization discrimination (XPD) level of 31.5 dB. However, the antenna profile has a high thickness of 6.6 mm, which is 1.32 wavelengths at the center frequency of 60 GHz. Moreover, the impedance bandwidth of the hollow-waveguide antenna is only 6.5%. In [8], excessive etching occurs during the milling process of thin metal plates, when a radiation slot layer is loaded into a traditional planar stacked antenna. Due to the presence of weak parts that are prone to break and cumb in the hollow-waveguide antenna prototype, the measured impedance bandwidth is only 3.3% and the efficiency is 50%. On the basis of [3], [9] improves the antenna performance, achieving a bandwidth of 19.2%, an efficiency of 86.6%, and an XPD level of 30 dB in the E-band. However, the complexity of the antenna design may lead to more machining errors, thereby increasing the uncertainty of measured results.

Continuous transverse stub array antennas are used for high XPD level and efficient linearly polarized antennas [10–12]. In [12], the 45° linearly polarized antenna consists of four layers: the feed network, cavity layer, radiating slots on continuous transverse stub, and 45° linear polarizer, achieving a high XPD level of 41 dB while maintaining an aperture efficiency of over 74%. But compared to [10], the linear polarizer adds two additional layers, resulting in increased profile and processing complexity.

In order to solve the complex structural problems mentioned and improve the antenna performance, researchers have replaced the antennas containing a complex feed network with a substrate-integrated waveguide (SIW) antenna array. The conventional way to achieve a 45° linearly polarized antenna is to etch the 45° inclined slots on the top metal layer of the SIW [13–16]. In [13], the 45° linearly polarized antenna using SIW technology is achieved through two layers of standard printed circuit boards (PCBs), which, however, suffers a narrow bandwidth of only 2.88%. In [14], a series slot coupling antenna by alternating inductive and capacitive loading is proposed to achieve low profile and small size. Unfortunately, the narrow antenna bandwidth can only cover 2.7%, and the XPD level is 13.81 dB, which requires other technologies to optimize, such as dielectric resonator antenna and coaxial line [15, 16]. In recent years, higher-order-mode cavities have been introduced in millimeter-wave antennas [17–19], due to their advantages of high efficiency and compact size. In fact, above 45° linearly polarized antennas do not use higher-order mode cavities. In [19], a 45° linear polarized antenna is achieved

© The Author(s), 2024. Published by Cambridge University Press in association with The European Microwave Association.

by TE_{170}-cavity-fed C-shaped patches with an efficiency of 98.9% and an XPD level of 20 dB. However, the impedance bandwidth is only 9.17%, which still needs to be improved.

This paper presents a method to achieve a 45° linear polarized 6×6 slot antenna array with high performance by means of asymmetric cross slots etched on the high-order-mode (HOM) cavity. The proposed antenna achieves broadband, high radiation efficiency, and high XDP level, while also having the advantages of simple structure and low profile. This paper is organized as follows. The 3×3 subarray design section describes the HOM cavity working principle and 3×3 subarray design. The 6×6 array design section presents the 6×6 antenna array, followed by the Conclusion section.

3×3 subarray design

The proposed 3×3 subarray is shown in Fig. 1. The subarray consists of one substrate layer and two metallic layers. The monolayer substrate is Rogers 5880 with a thickness of 1.575 mm. The asymmetric orthogonal slots with a length, width, and offset of 3 mm, 1.2 mm, and 0.25 mm are etched at the upper metal layer. The high-order mode TE_{330} in the square SIW cavity is excited by the coaxial feeding. The resonant frequency of the mode is given as follows:

$$f_{mnp} = \frac{c}{2\pi\sqrt{\mu\varepsilon}}\sqrt{(\frac{m\pi}{L_{\text{eff}}})^2 + (\frac{n\pi}{W_{\text{eff}}})^2 + (\frac{pm\pi}{h})^2}, \quad (1)$$

$$L_{\text{eff}} = L - \frac{d^2}{0.95p}, \qquad W_{\text{eff}} = W - \frac{d^2}{0.95p}, \quad (2)$$

where W, L, and h are the width, length, and height of the SIW cavity (SIWC) and d and p are the diameter and spacing of the SIW vias, respectively. The TE_{330} mode inside SIWC means $m = 3$, $n = 3$, and $p = 0$. The permeability and permittivityof the substrate μ and ε are 1 and 2.2, respectively. The electric field is determined by (3), where E_0 and ϕ are the amplitude and phase of the waves [20],

$$E_{Z,\,TE_{330}} = E_0 \sin\frac{3\pi x}{L_{\text{eff}}} \sin\frac{3\pi y}{W_{\text{eff}}} \cos(\omega t + \phi). \quad (3)$$

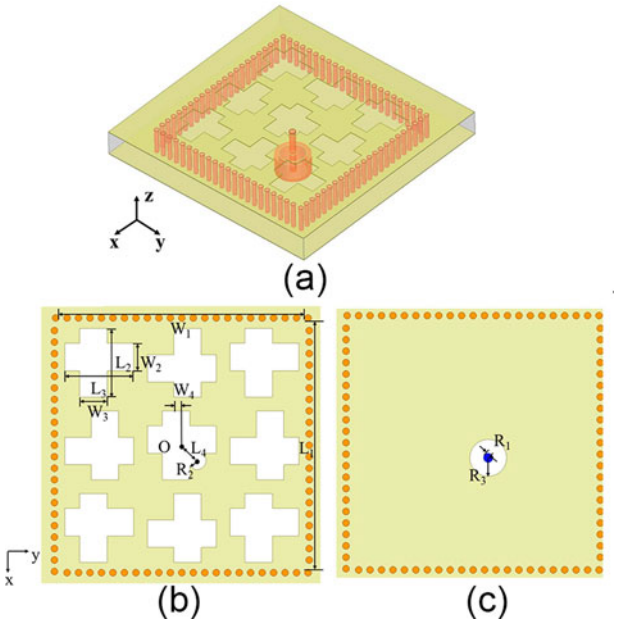


Figure 1. Subarray antenna: (a) over view, (b) top view, and (c) bottom view.

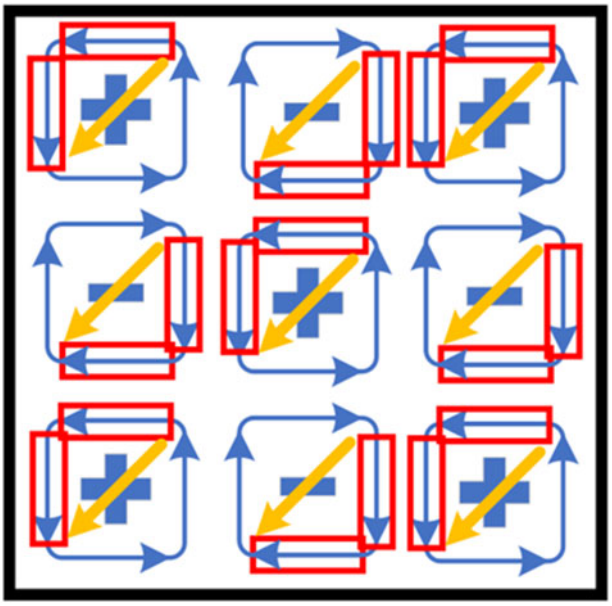


Figure 2. Electric field and magnetic vector of TE_{330} mode.

The 45° linear polarization is achieved by introducing asymmetric orthogonal slot radiation into the copper layer, which is on the top layer of the HOM cavity. To better explain the principle of the slot position by HOM cavity, the distribution diagram of electric and magnetic fields of the TE_{330} mode is shown in Fig. 2. The 3×3 standingwave electric peaks are evenly distributed inside the SIWC. The signs "+" and "−" represent the direction of the electric field. The closed curves indicate the magnetic vector, and its arrow direction is the vector direction. The offset transverse and the longitudinal slots with the same size are etched in each segment along the horizontal and vertical directions of the magnetic field vector. The electric field distributions at the radiation slots in this paper have the same phase. Due to the same size of the horizontal and vertical slots, the orthogonal components in the horizontal and vertical directions are of equal amplitude. A sum magnetic field vector can be formed, resulting in the radiation of 45 ° linearly polarized electromagnetic waves.

Note that the directions of the electric field in adjacent subsections are out of phase, and the directions of rotation of the magnetic field vector are opposite. Therefore, radiation in the same phase and same polarization requires etching a pair of orthogonal slots at positions with the same vector direction in each subsection. In the same way, −45° linear polarization can also be achieved in this way, and the diverse linear polarizations can be realized by designing this pair of the orthogonal slots into different size. Figure 3 illustrates the electric field distribution before and after etching the slots for the purpose of the effect of the asymmetric cross slots on the antenna radiation.

In order to achieve better antenna performance, it is necessary to determine the size of the cavity in the antenna and the mode excited within it. Figure 4 shows different antenna design and performance comparison using TE_{330} mode and TE_{340} mode.

https://doi.org/10.1017/S1759078724001028 Published online by Cambridge University Press

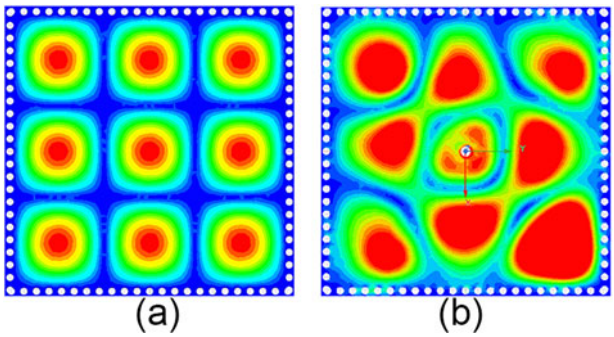


Figure 3. Electric field distribution at 39 GHz: (a) before etching slots and (b) after etching slots.

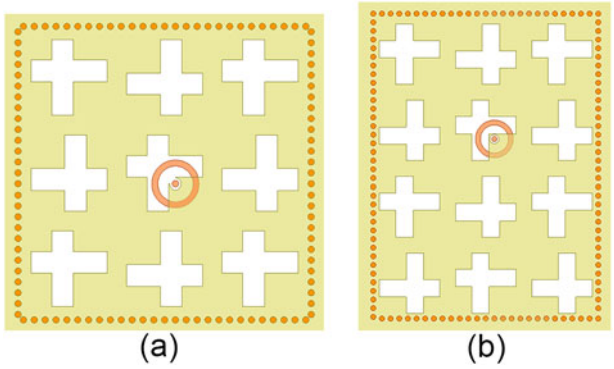


Figure 4. Subarray structures: (a) 3×3 and (b) 3×4.

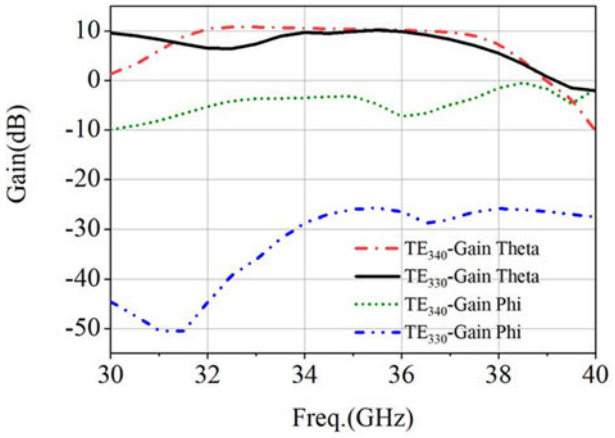


Figure 5. Radiation performance of the subarray of different resonant modes.

The antenna subarrays are arranged in two ways, 3×3 and 3×4. The size of the resonant cavity is calculated using (1), (2), and (3), as shown in Fig. 4. The offset of the feeding position, the size of the etching gap, and the offset value are kept consistent. From the simulation gain results of the E-plane (Phi = 45°) in Fig. 5, it can be seen that the antenna excited by TE_{330} mode has more advantages in XPD than the antenna excited by TE_{340} mode. In conclusion, for the 45° linearly polarized antenna in this paper, the cavity size has a significant impact on XPD. A square cavity can better form the 45° linearly polarized wave due to the consistent size of the metal walls, while the shape of a rectangular cavity can reduce the XPD. It is worth mentioning that when using an HOM cavity to achieve

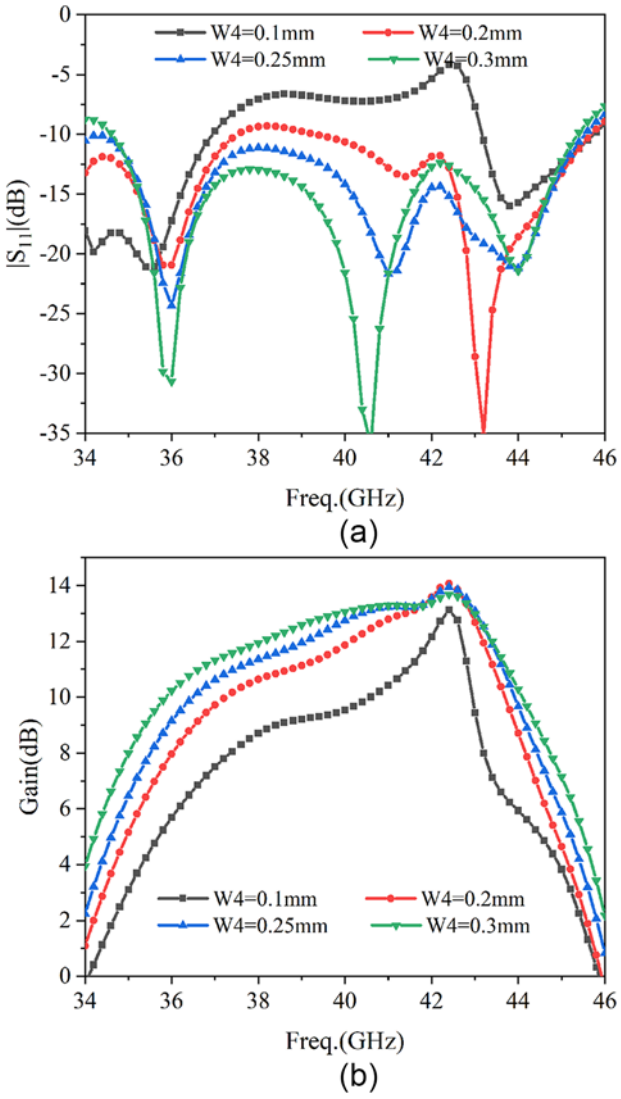


Figure 6. The influence of the slots offset of W4 on subarray performance: (a) *S*-parameter and (b) gain.

a compact design, we aim to use a single feed port to excite as many radiation slots as possible. On the other hand, we want to maintain a wide bandwidth. However, as the mode order increases, the bandwidth of the antenna decreases. This is because higher-order modes are more sensitive to the cavity size. Therefore, there is a trade-off between mode order and bandwidth.

In addition, W4 is the offset dimension between the center of the transverse slot and the center of the longitudinal slot. As depicted in Fig. 6, when W4 varies between 0.1 mm, 0.2 mm, 0.25 mm, and 0.3 mm, it is evident that both the antenna matching bandwidth and the gain increase with increasing W4. To ensure the impedance bandwidth ($|S_{11}| \leq -10$ dB) of the antenna, the value of W4 is chosen as 0.25mm.

R2 is the size of concentric circle etching on the outer side of the probe in the metal layer. It can be seen from Fig. 7 that when the antenna presents an upper metal electrical contact, R2 = R1 = 0.2 mm, it can be seen that the matching situation of the antenna is much worse than that without an electrical contact. In summary, electrical contact can cause impedance matching to deteriorate, and as the R2 increases, impedance matching will deteriorate,

https://doi.org/10.1017/S1759078724001028 Published online by Cambridge University Press

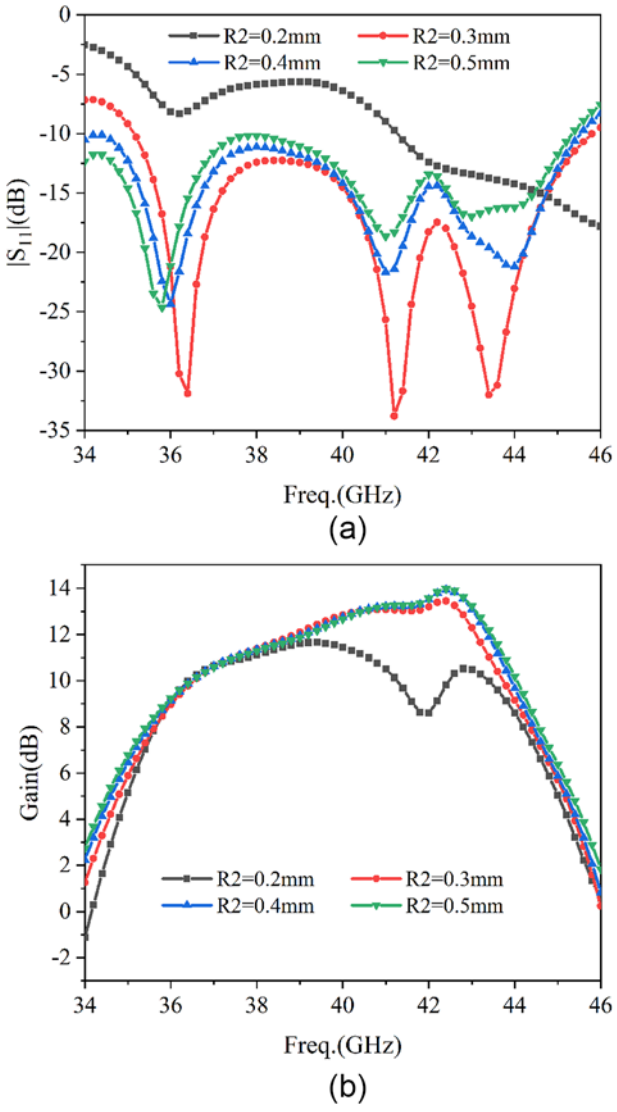


Figure 7. The influence of the R2 on subarray performance: (a) *S*-parameter and (b) gain.

Table 1. Dimensions of the subarray in millimeters.

Parameter	L1	L2	L3	W1	W2
Values	10.8	3	3	10.8	1.2
Parameter	W3	W4	R1	R2	R3
Values	1.2	0.25	0.2	0.4	0.81

resulting in an increase in low-frequency bandwidth. Therefore, selecting an appropriate etching size can effectively improve the working bandwidth of the antenna. So the value of R2 is chosen to be 0.4 mm.

The detailed parameters are shown in Table 1 with values in millimeters. The simulated results of the proposed 45° subarray are given in Fig. 8. As shown in Fig. 8, the subarray can achieve an impedance bandwidth of 27.8% (34.4–45.53 GHz) and a 3-dB gain bandwidth of 17.1% (36.88–43.76 GHz). The maximum gain is 13.5 dBi.

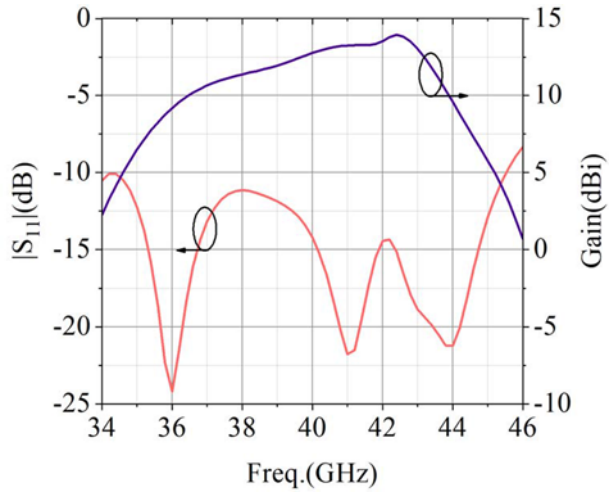


Figure 8. The S-parameter and peak gains in the broadside direction of the subarray antenna.

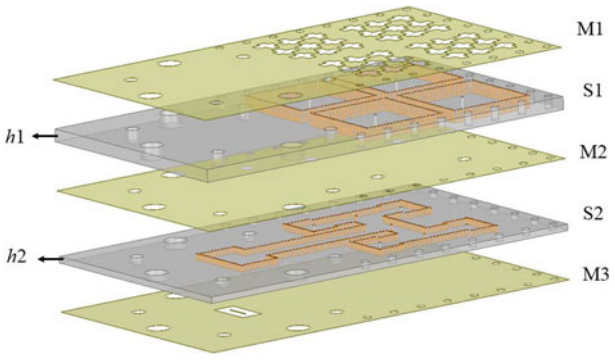


Figure 9. 3D exploded view of the proposed antenna array ($h1 = 1.515$ mm, $h2 = 0.787$ mm).

6×6 array design

Array design

Based on the structure of the proposed subarray, an exploded view of a 6×6 antenna array is shown in Fig. 9. Two PCB layers are used for array construction. The upper layer consists of 2×2 subarrays, with a spacing of 13.2 mm between each two subarrays. Figure 10(a) shows the feed network of the proposed antenna for TE_{330} mode excitation. The feed network is fed by a WR-22 waveguide, and a conversion to the probe (shown in Fig. 10(b)) is used at the end to feed the subarray. The substrate of the feeding network layer is Rogers 5880 with a thickness of 0.787 mm. As shown in Fig. 10(c), the simulated −15 dB $|S_{11}|$ bandwidths of the feed network and the transition structure cover 36–43.5 GHz. The transmission loss of the feednetwork is 0.16 dB, and the maximum difference among $|S_{12}|$, $|S_{13}|$, $|S_{14}|$, and $|S_{15}|$ is below 0.44 dB within the operation bandwidth.

In the M2 layer, a larger concentric circle at the location of the probe is etched for better impedance matching. The part outside the cavity is loaded with through holes for mounting screws, in order to reduce the performance deteriation caused by the air gap between two PCBs. The feeding network design parameters and values are shown in Fig. 10.

https://doi.org/10.1017/S1759078724001028 Published online by Cambridge University Press

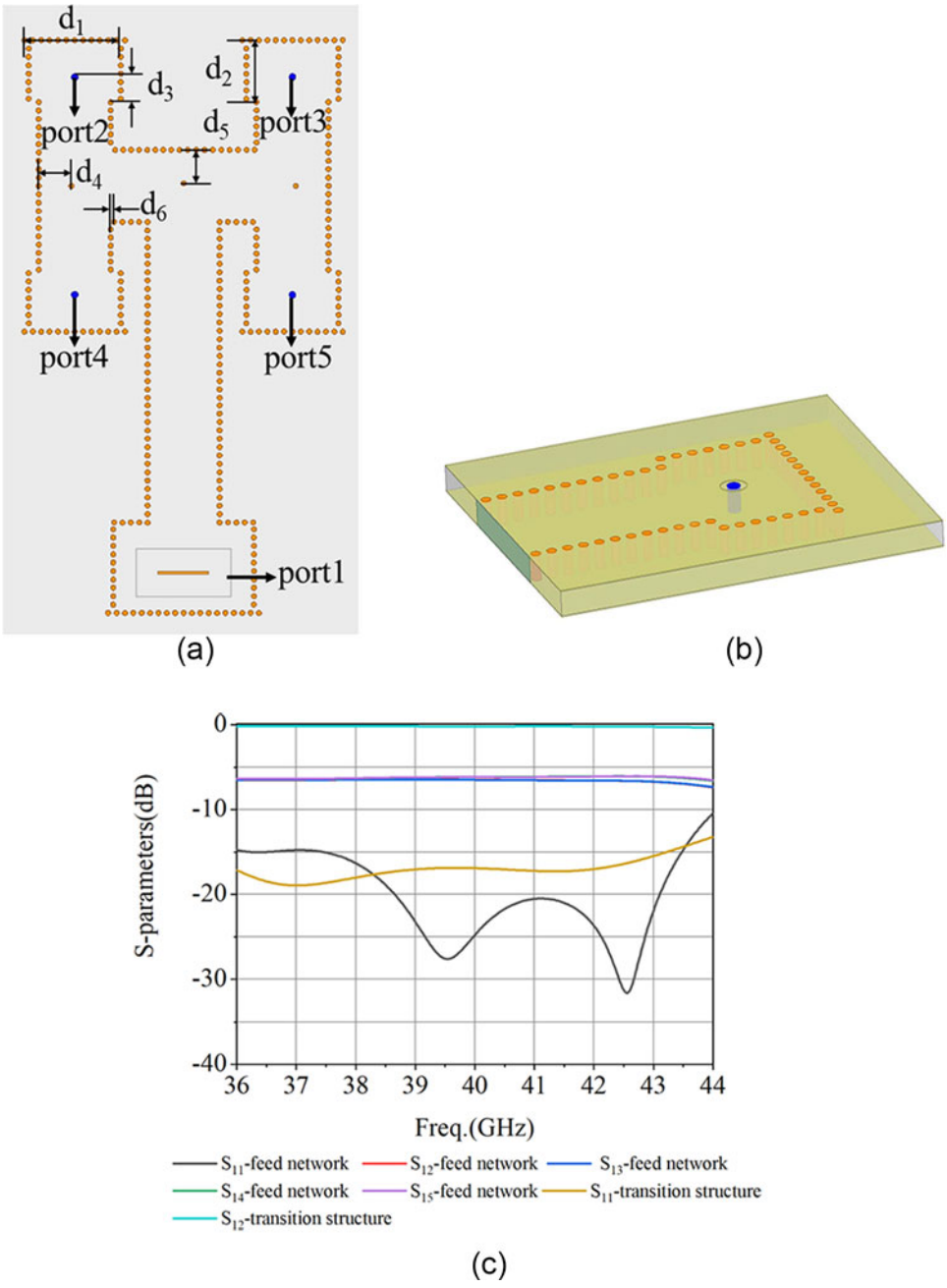


Figure 10. (a) Structure of the feed network for TE_{330} mode. (b) Transition structure from SIW to probe. (c) Their properties in simulations (*d1* = 5.5 mm, *d2* = 3.83 mm, *d3* = 1.7 mm, *d4* = *d5* = 1.8 mm, *d6* = 0.2 mm).

Results and discussion

Figure 11 shows the images of the 6×6 antenna array prototype and the array in the test environment. The antenna was fabricated using standard PCB technology. The antenna array has the dimensions of 53 mm×30 mm×2.432 mm and the aperture area of 21.6 mm×21.6 mm surrounded by screw holes for assembly. In Fig. 12(a), the simulated and measured *S*-parameters of the 6×6 antenna array for $|S_{11}| \leq -10$ dB are 15.3% (36.89–43 GHz) and 13.9% (36.98–42.52 GHz), respectively.

The antenna was measured using a spherical near-field measurement system. In Fig. 12(b), the simulated and measured peak gain is 19.06 dBi and 19.3 dBi, respectively. The simulated 3-dB gain bandwidth is 16.02% (36.85–43.31 GHz), and the measured one is 13.6% (37–42.4 GHz). The measured aperture efficiency is 88.1% at 38.5 GHz, and the average measured aperture efficiency is 66.9%. The simulated radiation efficiencies are above 86.5% within the impedance bandwidth, and the maximum radiation efficiency can reach 91.7% at 39 GHz. The average measured radiation efficiency is 75%. The discrepancies in the measured results are due to the fact that the antenna test environment is not ideal, in which the placement and the test accuracy need to be improved.

The simulated and measured radiation patterns in $-90^\circ < \theta < 90^\circ$ are given in Fig. 13. The XPD levels in the maximum radiation

https://doi.org/10.1017/S1759078724001028 Published online by Cambridge University Press

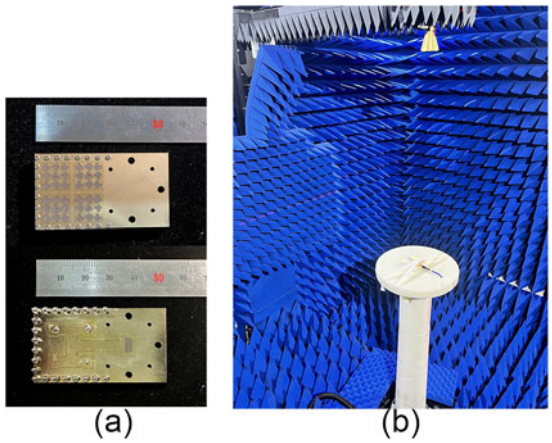


Figure 11. (a) The image of the fabricated prototype. (b) Measurement environment of the antenna.

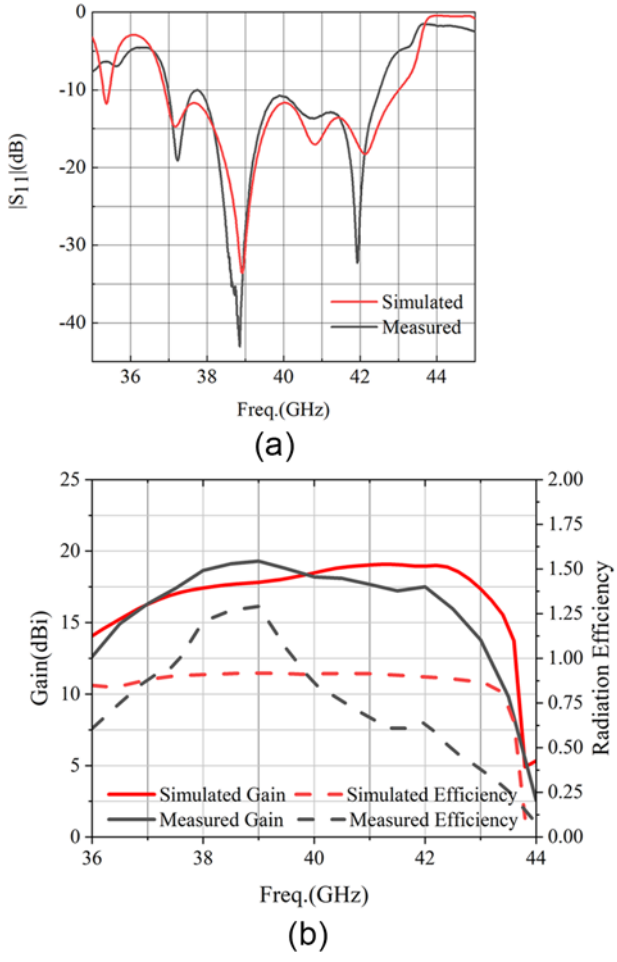


Figure 12. Measured and simulated results of the antenna array. (a) $|S_{11}|$ and (b) gain and radiation efficiency.

direction are higher than 30 dB at 38, 40, and 42 GHz, indicating good 45° linear polarization characteristic.

There are many papers that aimed at the 45° linear polarized antenna, and a comparison is made in Table 2. Compared to other SIW technology-based 45° linearly polarized antennas, the proposed antenna etching asymmetric cross slots on the top layer of

Table 2. Comparision with other 45° LP antennas

Ref.	Antenna type	Freq. (GHz)	IBW (%)	Peak gain (dBi)	RE (%)	AE (%)	No. of elements	Total size (λ^3)	XPD (dB)
[15]	SIW + DR	35	6.25	13.55	85	49.7	1×8	6.31×8.42×0.618	N.A.
[19]	SIW + patch	34.5	9.71	14.1	98.9*	91.5	1×7	4.65×3.34×0.284	20
[21]	SIW + patch	79	10.6	17.2	52.4	N.A.	2×8	N.A.×N.A.×0.067	<20
[22]	SIW + rod	60	13.2	17.5	N.A.	49.9	4×4	3.2×2.8×5.1(CS)	18
[23]	HW + slot	28.5	31.58	26.1	88.8	87.7	8×8	7.03×7.03×1.748	45.8
[24]	HW + slot	28	18.8	25	71.7	61	8×8	7.02×7.02×0.933	31.3
This paper	SIW + slot	39	13.9	19.3	75#	66.9#	6×6	6.89×3.9×0.316	30

IBW: relative impedance bandwidth; RE: radiation efficiency; AE: aperture efficiency; XPD: cross-polarization discrimination level at $\theta = 0°$; HW: hollow-waveguide; DR: dielectric resonator; *: simulated results; N.A.: not apply; CS: cavity size; #:Average value within the working band

https://doi.org/10.1017/S1759078724001028 Published online by Cambridge University Press

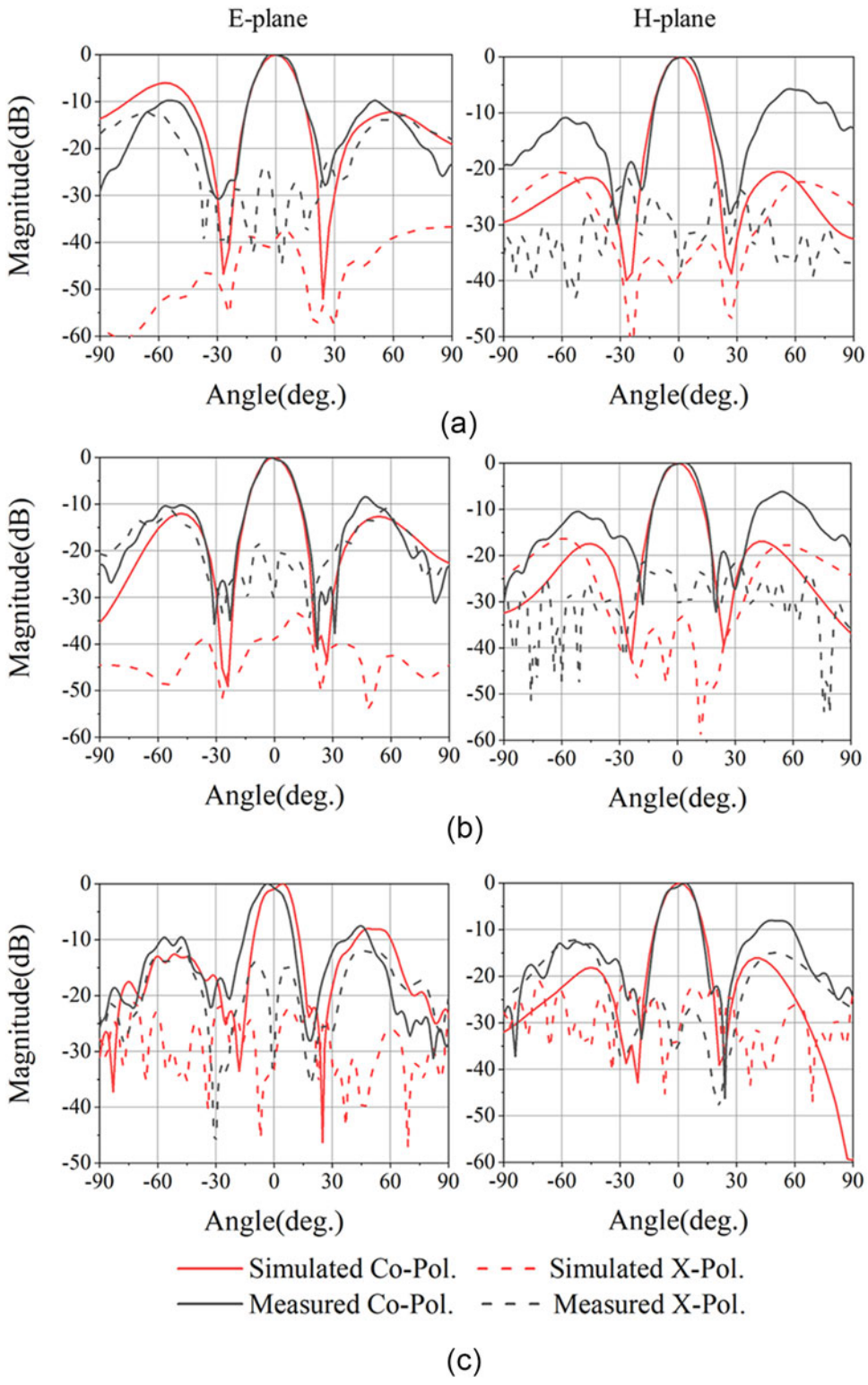


Figure 13. Simulated and measured radiation patterns in E-plane ($\phi = 45°$) and H-plane ($\phi = 135°$): (a) 38 GHz, (b) 40 GHz, and (c) 42 GHz.

HOM cavity is more dominant in terms of bandwidth and XDP level, which is better than that in [15, 19, 21] and is comparable to that in [22]. However, [22] has a wide impedance bandwidth at the expense of the profile. Meanwhile, [23] and [24] are slot array antennas fed by hollow-waveguide, which have wide impedance bandwidths and high XPD levels, but the profiles are higher than the proposed antenna. What is more, the radiation efficiency is higher than that in [24].

https://doi.org/10.1017/S1759078724001028 Published online by Cambridge University Press

Conclusion

In this paper, a wideband and high XPD level 45° linearly polarized antenna array has been designed. Asymmetric orthogonal slots etched on the top of the high-order mode cavity contributes to low profile and wide bandwidth. Compared to the waveguide-fed antenna, the proposed antenna has the advantages in profile and radiation efficiency. In conclusion, the characteristics of the 45° linear polarized antenna show more potential in 5G communications.

Acknowledgements. This work was supported in part by the project of 2022YFF0604200 from that National Key R&D Program of China and in part by the project of 62301065 from the National Natural Science Foundation of China.

Competing interests. The author(s) declare none.

References

1. **Ullah H and Tahir FA** (2020) A high gain and wideband narrow-beam antenna for 5G millimeter-wave applications. *IEEE Access* **8**, 29430–29434.
2. **Zhu J, Liao S, Li S and Xue Q** (2018) 60 GHz substrate-integrated waveguide-based monopulse slot antenna arrays. *IEEE Transactions on Antennas and Propagation* **66**(9), 4860–4865.
3. **Tomura T, Miura Y, Zhang M, Hirokawa J and Ando M** (2012) A 45° linearly polarized hollow-waveguide corporate-feed slot array antenna in the 60-GHz band. *IEEE Transactions on Antennas and Propagation* **60**(8), 3640–3646.
4. **Guo J, Hu Y and Hong W** (2022) A 45° polarized wideband and wide-coverage patch antenna array for millimeter-wave communication. *IEEE Transactions on Antennas and Propagation* **70**(3), 1919–1930.
5. **Zhong J AK Rashid and Q Zhang** (2020) 45° linearly polarized and circularly polarized high-scanning-rate leaky-wave antennas based on slotted substrate integrated waveguide. *IEEE Access* **8**, 82162–82172.
6. **Hong W** (2017) Multibeam antenna technologies for 5G wireless communications. *IEEE Transactions on Antennas and Propagation* **65**(12), 6231–6249.
7. **Ding C and Luk KM** (2022) Wideband omnidirectional circularly polarized antenna for millimeter-wave applications using conformal artificial anisotropic polarizer. *IEEE Transactions on Antennas and Propagation* **70**(4), 2450–2458.
8. **Garcia-Marin E, Masa-Campos JL and Sanchez-Olivares P** (2018) Diffusion bonding manufacturing of high gain W-band antennas for 5G applications. *IEEE Communications Magazine* **56**(7), 21–27.
9. **Tomura T, Hirokawa J, Hirano T and Ando M** (2014) A 45° linearly polarized hollow-waveguide 16 ×16-slot array antenna covering 71–86 GHz band. *IEEE Transactions on Antennas and Propagation* **62**(10), 5061–5067.
10. **Foglia FM** (2019) A wide-angle scanning switched-beam antenna system in LTCC technology with high beam crossing levels for V-band communications. *IEEE Transactions on Antennas and Propagation* **67**(1), 541–553.
11. **Lu Y, You Q, Wang Y, You Y, Huang J and Wu K** (2018) Millimeter-wave low-profile continuous transverse stub arrays with novel linear source generators. *IEEE Transactions on Antennas and Propagation* **67**(2), 988–997.
12. **You Y** (2019) High-performance E-band continuous transverse stub array antenna with a 45° linear polarizer. *IEEE Antennas and Wireless Propagation Letters* **18**(10), 2189–2193.
13. **Dong-yeon K, Chung W, Changhyun P, Lee S and Nam S** (2012) A series slot array antenna for 45 °-inclined linear polarization with SIW technology. *IEEE Transactions on Antennas and Propagation* **60**(4), 1785–1795.
14. **Dong-yeon K, Chung W, Changhyun P, Lee S and Sangwook N** (2011) Design of a 45°-inclined SIW resonant series slot array antenna for Ka-band. *IEEE Antennas and Wireless Propagation Letters* **10**, 318–321.
15. **Abdallah MS, Wang Y, Abdel-Wahab WM and Safavi-Naeini S** (2018) Design and optimization of SIW center-fed series rectangular dielectric resonator antenna array with 45° linear polarization. *IEEE Transactions on Antennas and Propagation* **66**(1), 23–31.
16. **Liu B** (2018) A 45° linearly polarized slot array antenna with substrate integrated coaxial line technique. *IEEE Antennas and Wireless Propagation Letters* **17**(2), 339–342.
17. **Zhao W, Li X, Qi Z and Zhu H** (2021) High-order-mode cavity fed antenna arrays for diverse polarizations with compact size, high gain, and high efficiency. *IEEE Transactions on Antennas and Propagation* **70**(2), 1045–1056.
18. **Zhao W, Li X, Qi Z and Zhu H** (2022) Broadband and high-gain high-order-mode fed open-ended waveguide antenna array for millimeter-wave applications. *IEEE Transactions on Antennas and Propagation* **70**(9), 8614–8619.
19. **Chen SL, Wu GB, Wong H and Chen BJ** (2022) Millimeter-wave slot-based cavity antennas with flexibly-chosen linear polarization. *IEEE Transactions on Antennas and Propagation* **70**(8), 6604–6616.
20. **Pozar D** (2013) *Microwave Engineering*. New York, NY: John Wiley & Sons, 4th Edn.
21. **Yu Y, Hong W, Jiang ZH and Zhang H** (2018) E -band low-profile, wideband 45° linearly polarized slot-loaded patch and its array for millimeter-wave communications. *IEEE Transactions on Antennas and Propagation* **66**(8), 4364–4369.
22. **Guntupalli AB and Wu K** (2014) 45° linearly polarized high-gain antenna array for 60-GHz radio. *IEEE Antennas and Wireless Propagation Letters* **13**, 384–387.
23. **Zhou H, Lu Y, You Q, Wang Y and Huang J** (2022) Wideband and high cross-polarization discrimination 45° linearly polarized slot array antenna without cavity-backed layer. *IEEE Antennas and Wireless Propagation Letters* **21**(10), 2005–2009.
24. **You Y, Lu Y, Skaik T, Wang Y and Huang J** (2021) Millimeter-wave 45° linearly polarized corporate-fed slot array antenna with low profile and reduced complexity. *IEEE Transactions on Antennas and Propagation* **69**(9), 6064–6069.



Yutong Yang received the B.E. degree in electronic information science and technology from Xidian University, Xian, China, in 2021. She is currently pursuing the M.S. degree in electronic science and technology from that Beijing University of Posts and Telecommunications. Her current research interests include characteristic modes theory and millimeter-wave antennas.



Zihang Qi received the B.E. degree in electronic and information engineering from China Three Gorges University, Yichang, China, in 2013, and the Ph.D. degree in electronic science and technology from the Beijing University of Posts and Telecommunications, Beijing, China, in 2019. He is currently an associate research fellow with the Beijing University of Posts and Telecommunications. His current research interests include orbital angular momentum antennas, millimeter-wave/THz antennas, and microwave filters.



Wenyu Zhao received the B.S. degree and Ph.D degree from the Beijing University of Posts and Telecommunications, Beijing, China, in 2018 and 2023, respectively. He is currently a postdoctoral researcher with the School of Electronic Engineering and the Beijing Key Laboratory of Work Safety Intelligent Monitoring in the Beijing University of Posts and Telecommunications. His current research interests include high-order-mode antennas, millimeter-wave antennas, and metasurface antennas.

https://doi.org/10.1017/S1759078724001028 Published online by Cambridge University Press



Genqiang Kou received the B.E. degree in electronic information science and technology from Beijing University of Posts and Telecommunications, Beijing, China, in 2021. He is currently pursuing the M.S. degree in electronic science and technology from the Beijing University of Posts and Telecommunications. His current research interests include high-order-mode antennas and millimeter-wave antennas.



Xiuping Li received the B.S. degree from Shandong University in 1996, and the Ph.D. degree from the Beijing Institute of Technology in 2001. From 2001 to 2003, she joined in Positioning and Wireless Technology Center, Nanyang Technological University, where she was a research fellow and involved in the research and development of Radio Frequency Identification (RFID) system. In 2003, she was a research professor in Yonsei University, South Korea. Since 2004, she joined Beijing University of Posts and Telecommunications as an associate professor and promoted to professor in 2009. She has been selected into the New Century Excellent Talents Support Plan in National Ministry of Education, the Beijing Science and Technology Nova Support lan. She won the second prize of the Progress in Science and Technology of China Institute of Communications and the Excellent Achievements in Scientific Research of Colleges and Universities. Her research interests include millimeter-wave antennas, THz antennas, RFID systems, and Monolithic Microwave Integrated Circuit (MMIC) design.

https://doi.org/10.1017/S1759078724001028 Published online by Cambridge University Press